Enhanced pathogenicity and neurotropism of mouse-adapted H10N7 influenza virus are mediated by novel PB2 and NA mutations

Xuxiao Zhang,[a] Guanlong Xu,[b] Chenxi Wang,[a] Ming Jiang,[a] Weihua Gao,[a] Mingyang Wang,[a] Honglei Sun,[a] Yipeng Sun,[a] Kin-Chow Chang,[c] Jinhua Liu,[a] and Juan Pu[a]*

Key Laboratory of Animal Epidemiology and Zoonosis, Ministry of Agriculture, College of Veterinary Medicine, and State Key Laboratory of Agrobiotechnology, China Agricultural University, Beijing, China[a]. China Institute of Veterinary Drug Control, Beijing, China[b]. School of Veterinary Medicine and Science, University of Nottingham, Sutton Bonington Campus, Loughborough, United Kingdom[c].

Running title: Pathogenicity and neurotropism of H10N7 virus in mice

* Address correspondence to Juan Pu, pujuan@cau.edu.cn.

Word counts: Abstract: 238; Main text: 4151.

Abstract

Recent human fatalities from avian-origin H10N8 influenza virus infection raise concerns about the threat of this virus subtype to public health. To investigate genetic adaptation of H10 avian influenza viruses in mammals, we generated a mouse-adapted avian H10N7 variant (A/mallard/Beijing/27/2011-MA, [BJ27-MA]) through nine serial passages in mice. Mice infected with BJ27-MA virus died by 6 days post-infection and showed neuronal infection in contrast to parental virus which elicited no overt symptoms. Sequence analysis showed the absence of the widely recognized mammalian adaptation markers of E627K and D701N in PB2 in the mouse-adapted strain; instead five amino acid mutations were identified: E158G and M631L in PB2, G218E in HA (H3 numbering), and K110E and S453I in NA. Neurovirulence of BJ27-MA virus necessitated the combined presence of the PB2 and NA mutations. Mutations M631L and E158G of PB2 and K110E of NA were required to mediate increased virus replication and severity of infection in mice and mammalian cells. PB2-M631L was functionally the most dominant mutation in that it strongly up-regulated viral polymerase activity and played a critical role in the enhancement of virus replication and disease severity in mice. K110E mutation in NA, on the other hand, significantly promoted NA enzymatic activity. These results indicate that the novel mutations in PB2 and NA genes are critical for the adaptation of avian H10N7 influenza virus in mice, which could serve as molecular signatures of virus transmission to mammalian hosts including humans.

Importance

The increasingly prevalent H10 subtype of avian influenza virus in China has recently been a source of human fatalities. We demonstrated that an avian H10N7 virus can readily be adapted to become highly pathogenic and neurotropic in mice. Mutations in PB2 and NA from the mouse-adapted virus (BJ27-MA) were the major determinants of enhanced pathogenicity of which mutation PB2-M631L was functionally most dominant. Although BJ27-MA virus lacked the well-known mammalian adapted mutations (namely PB2-E627K and PB2-D701N), PB2-M631L mutation enhanced viral polymerase activity, replication and pathogenicity of BJ27-MA virus in mice, indicating a novel adaptation strategy. These observations affirm the public health threat of avian H10 subtype influenza viruses and have implications in the assessment of potential mutant viruses that may cause severe infections in humans.

Introduction

Presently, avian influenza viruses (AIVs) cause great economic losses to the global poultry industry, which historically were major contributors to the 1918 H1N1, 1957 H2N2 and 1968 H3N2 virus pandemics (1). H5N1 and H9N2 influenza viruses, as the two principal subtypes circulating in poultry, are high on the list of candidates that could potentially cause another major human influenza outbreak (2, 3). However, recent human cases of emergent avian H7N9 virus infection challenge our understanding of the main subtypes of possible future pandemic human virus (4). Thus, contingency planning in the prevention and management of avian influenza virus infections in human should be based on a broad range of possible subtypes.

Between November 2013 and February 2014, two fatal and one severe cases of human infections with a novel reassortant H10N8 virus in Jiangxi, China, were reported for the first time (5-7). Avian H10 virus subtype was firstly isolated from chickens in Germany in 1949 (8, 9); subsequently viruses bearing H10 hemagglutinin (HA) and different neuraminidase (NA) subtypes have become widely prevalent in wild birds and domestic poultry around the world (10-12). Since 1984, repeated infections or deaths of mammals with this subtype have been reported, such as the outbreaks of H10N4 virus in minks (13), H10N5 virus in domestic pigs (14), H10N8 virus in feral dogs (15) and H10N7 virus in harbor seals (16-18). Human cases of H10 virus infections had occurred sporadically in several other countries. For example, H10N7 viruses had caused a number of human infections in Egypt in 2004 (19). In March 2010, H10N7 virus infection was identified in two abattoir workers in a

commercial poultry farm in Australia who showed conjunctivitis and minor upper respiratory tract symptoms (12). In the USA, serological evidence of exposure to H10 virus subtype was confirmed in turkey workers (20). The repeated human cases of H10 virus infections coupled with the prevalence of H10 viruses in birds raise concerns that this particular subtype could pose increasing threat to human and animal health. However, the molecular adaptations of H10 influenza viruses in mammals are largely unknown.

Adaptation is considered to be a primary driver in evolution, and the process of natural selection of influenza A viruses in experimental mice appears also to hold true for humans (21). Several adaptation studies of human H3N2, pandemic 2009 H1N1, avian H9N2 and H6N6 influenza viruses in mice have provided better understanding of molecular determinants of virus pathogenicity in mammals including humans (22-26). Here, to explore the genetic adaptations of H10 AIV subtype in mammals, we serially passaged a low-pathogenicity avian-derived H10N7 virus in mice. We found that mouse-adapted H10N7 virus acquired high pathogenicity status causing fatal infection and neurovirulence. The well-known mammalian adaptation markers PB2-E627K and PB2-D701N (27, 28) were not found in the mouse-adapted strain, but amino acid substitution PB2-M631L was a dominant contributor to virus virulence.

Materials and methods

Ethics statement

All animal work was approved by the Beijing Association for Science and

Technology (approval ID SYXK [Beijing] 2007-0023) and conducted in accordance with the Beijing Laboratory Animal Welfare and Ethics guidelines, as issued by the Beijing Administration Committee of Laboratory Animals, and in accordance with the China Agricultural University Institutional Animal Care and Use Committee guidelines (ID: SKLAB-B-2010-003).

Viruses and cells

The H10N7 virus A/mallard/Beijing/27/2011 (BJ27) was isolated in Beijing, China and propagated in the allantoic cavities of 10-day-old specific-pathogen-free (SPF) embryonated chicken eggs (Merial, Beijing, China) at 37°C for 72 h. Allantoic fluid containing virus was harvested, aliquoted and frozen at -80°C for later use. Viruses were titrated in MDCK cells to determine the 50% tissue culture infectious dose ($TCID_{50}$) by the Reed and Muench method (29). Human embryonic kidney (293T), human pulmonary adenocarcinoma (A549), Madin Darby canine kidney (MDCK) and mouse neuroblastoma N2a (N2a) cells were maintained in Dulbecco's modified Eagle's medium (DMEM, Gibco) supplemented with 10% fetal bovine serum (FBS, Gibco), 100 units/ml of penicillin, and 100 μg/ml of streptomycin at 37°C in 5% CO_2 atmosphere.

Adaptation of the BJ27 virus in mice

Six 6-week-old female BALB/c mice (Beijing Experimental Animal Center) were anesthetized with Zoletil 50 (tiletamine-zolazepam; Virbac S.A., Garros, France) and inoculated intranasally with 50 μl of allantoic fluid containing BJ27 virus. At 3 days post-inoculation (dpi), three mice were euthanized and the lungs were harvested and

125 homogenized in 1 ml of sterile cold phosphate-buffered saline (PBS). The
126 homogenate was centrifuged at 6,000 × g for 5 min at 4°C and filtered through a
127 0.22-μm-pore-size cellulose acetate filter (Millipore, USA). Fifty μl of filtered
128 homogenate were used as inoculum per mouse for the next passage (passage 2 [P2]).
129 The remaining three mice were monitored daily for clinical symptoms. At 9 passages
130 (P9), the virus in the lung homogenate was subjected to three rounds of plaque
131 purification in MDCK cells, and the cloned virus, designated BJ27-MA, was
132 amplified once in 10-day-old SPF embryonated eggs for 72 h at 37°C, as previously
133 described (30).

134 **Sequence analysis**

135 Viral RNA was extracted from allantoic fluid containing plaque-purified BJ27-MA.
136 The eight virus genes were amplified by reverse transcription-PCR (RT-PCR) and
137 sequenced. Adaptive mutations arising from serial passage were identified by
138 comparing consensus BJ27-MA and wild type BJ27 sequences.

139 **Plasmid construction and virus rescue**

140 The eight gene segments of BJ27 and BJ27-MA were amplified by RT-PCR and
141 cloned into the expression plasmid, PHW2000. Mutations of interest in the PB2, HA
142 and NA gene were introduced by PCR-based site-directed mutagenesis with primer
143 pairs containing point mutations. All constructs were sequenced to confirm mutational
144 changes.

145 Reassortant viruses between BJ27 and BJ27-MA were generated by reverse
146 genetics as described previously (31). Briefly, 0.5 μg of each gene segment plasmid

was mixed together and incubated with 8 μl of TransIT-LT1 reagent (Mirus Bio, USA) at 20°C for 30 min. The TransIT-LT1-DNA mixture was transferred to 70% confluent 293T/MDCK co-cultured monolayers and incubated at 37°C with 5% CO_2. Six hours post-transfection, the supernatants were replaced with 2 ml of Opti-MEM containing 2 μg/ml TPCK-treated trypsin (Sigma-Aldrich). Forty-eight hours post-transfection, the cell supernatants were harvested and inoculated into 10-day-old SPF embryonated eggs and incubated for 72 h at 37°C to prepare a virus stock. Viral RNA was extracted and analyzed by RT-PCR, and each viral segment was sequenced to confirm identity. Virus titers were determined by $TCID_{50}$ assay on MDCK cells.

Mouse experiments

Groups of eleven 6-week-old female BALB/c mice (Beijing Experimental Animal Center) were anesthetized with Zoletil 50 (tiletamine-zolazepam; Virbac S.A., Garros, France) and inoculated intranasally with $10^{5.5}$ $TCID_{50}$ of viruses in 50 μl PBS. Three mice in each group were euthanized at 3 and 5 dpi; lungs, brains, spleens, kidneys and livers were collected for virus titration in MDCK cells. The remaining five mice in each group were monitored for weight loss and mortality for 14 days. Mice that lost more than 30% of their body weight were humanely euthanized. To determine the fifty percent mouse lethal dose (MLD_{50}), groups of three 6-week-old female mice anesthetized with Zoletil 50 and inoculated intranasally with 50 μl of 10-fold serial dilutions of viruses in PBS. The mice were monitored for 14 days. MLD_{50} was calculated and expressed in $TCID_{50}$. For histopathology and immunohistological analysis, mouse lungs and brains collected at 5 dpi were fixed in 10%

phosphate-buffered formalin, embedded in paraffin, then cut into 5 mm-thick sections and stained with haematoxylin and eosin (H&E) or immunostained with a mouse monoclonal antibody specific for influenza A virus NP (Biorbyt, UK).

Viral growth kinetics

Selected recombinant viruses were inoculated onto MDCK cell monolayers (at multiplicity of infection [MOI] of 0.01), A549 cell monolayers (at MOI of 0.1) or N2a cell monolayers (at MOI of 0.1) in serum-free DMEM containing 1 μg/ml TPCK-treated trypsin and incubated at 37°C with 5% CO_2 atmosphere. Cell supernatants were harvested at 12, 24, 36, 48, 60 and 72 hours post-inoculation (hpi) and titrated on MDCK cells in 96-well plates. Three independent experiments were performed for each virus.

Polymerase activity assay

The PB2, PB1, PA and NP gene segments of BJ27, BJ27-MA and BJ27-PB2 mutants were individually inserted into pCDNA3.1 plasmid. PB2, PB1, PA and NP plasmids (125 ng each) were transfected to sixty percent confluent 293T cells, together with fire-fly luciferase reporter plasmid pYH-Luci (10 ng) and internal control plasmid expressing renilla luciferase (2.5 ng). After 24 hours of transfection, cell lysate was prepared with Dual Luciferase Reporter Assay System (Promega) and luciferase activity was measured using GloMax 96 microplate luminometer (Promega).

Western blotting

PB2 expression levels in different transfection groups were determined by Western

191 blotting. Total cell protein lysates were extracted from transfected 293T cells with
192 CA630 lysis buffer (150 mM NaCl, 1% CA630 detergent, 50 mM Tris base [pH 8.0]).
193 Cellular proteins were separated by 12% sodium dodecyl sulfate-polyacrylamide gel
194 electrophoresis (SDS-PAGE) and transferred to a polyvinylidenedifluoride (PVDF)
195 membrane (Amersham Biosciences, Germany). Each PVDF membrane was blocked
196 with 0.1% Tween 20 and 5% nonfat dry milk in Tris-buffered saline and subsequently
197 incubated with a primary antibody. Primary antibodies used were specific for
198 influenza A virus PB2 (ThermoFisher, USA) and β-actin (Beyotime, China).
199 Secondary antibody was horseradish peroxidase (HRP)–conjugated anti-rabbit or
200 -mouse antibody (Beyotime, China). HRP presence was detected using a Western
201 Lightning chemiluminescence kit (Amersham Pharmacia, Freiburg, Germany),
202 following the manufacturer's protocols.

203 **Neuraminidase (NA) activity assay with substrate 4-MU-NANA**

204 NA activity assays using the soluble substrate MUNANA (Sigma, Germany) were
205 performed as previously described (32). Briefly, virus was diluted to 10^6 $TCID_{50}$/ml
206 and 50 μl was added to each well of a black 96-well plate (CoStar). Concentrations of
207 MUNANA substrate ranging from 2.0 μM to 200 μM were used. When cleaved by
208 the viral NA, MUNANA produces a fluorescent product. Fluorescence was quantified
209 using a Biotek Synergy H1 plate reader every 3 minutes over the course of 45 minutes.
210 Fluorescence curves were then fitted to the Michaelis-Menton equation to determine
211 values of V_{max} and K_m. Each experiment comprised triplicate samples of each virus.

212 **Statistical analyses**

All statistical analyses were performed using GraphPad Prism Software Version 5.00 (GraphPad Software Inc., San Diego, CA, USA). Statistically significant differences between experimental groups were determined using the analysis of variance (ANOVA). Differences were considered statistically significant at $P < 0.05$.

Nucleotide sequence accession numbers

The nucleotide sequences of the eight gene segments of H10N7 are available from GenBank under accession numbers: KX898962 for PB2, KX898963 for PB1, KX898964 for PA, KX898965 for HA, KX898966 for NP, KX898967 for NA, KX898968 for M, and KX898969 for NS.

Results

Adaptation of avian H10N7 influenza virus in mice

To mimic the adaptation of avian H10 subtype influenza virus in mammalian hosts, A/mallard/Beijing/27/2011 H10N7 virus (BJ27) was serially passaged in murine host by intranasal inoculation of $10^{5.5}$ $TCID_{50}$ of virus per mouse. Mice at passage 1 (P1) infected with wild type BJ27 did not show overt clinical sign. At P5, infected mice showed mild clinical signs, including decreased activity and ruffled coat. At P9 and P10, mice displayed severe clinical symptoms of respiratory distress, inactivity and inappetence; all infected mice died by 5 dpi (data not shown), indicating significant increase in pathogenicity. P9 virus from lung homogenate was plaque purified three times in MDCK cells and designated BJ27-MA.

Mouse-adapted H10N7 virus exhibited enhanced pathogenicity and neurovirulence

BALB/c mice were infected, in two groups of eleven mice each, with $10^{5.5}$ $TCID_{50}$ of BJ27 or BJ27-MA virus to compare virus pathogenicity. BJ27-MA virus caused

238 dramatic weight loss in infected mice and all were dead by 6 dpi, while mice infected
239 with BJ27 showed modest weight loss of 8.7% and recovery weight gain from 7 dpi
240 (Fig. 1A and B). To determine whether the differences in pathogenicity between BJ27
241 and BJ27-MA virus were due to altered virus replication, groups of three BALB/c
242 mice were euthanized at 3 and 5 dpi respectively, and virus titers in lung and brain
243 were determined. As shown in Fig 1C and D, mouse-adapted BJ27-MA virus
244 replicated to higher titers in the lungs than wild type BJ27 virus at 3 and 5 dpi.
245 Furthermore, BJ27-MA virus was isolated from brains of infected mice in rising titers
246 from mean titer of 2.1 $\log_{10}$ $TCID_{50}$ /ml at 3 dpi to 2.8 $\log_{10}$ $TCID_{50}$ /ml at 5 dpi. No
247 virus was isolated from brains of BJ27 virus infected mice. Therefore, the
248 mouse-adapted BJ27-MA virus has acquired neurotropism which would have
249 contributed to the severity of infection in mice.

250 **Genetic changes in adapted BJ27-MA virus**

251 To identify potential segments and amino acid substitutions that are responsible for
252 increased pathogenicity and replication of BJ27-MA virus in mice, the consensus
253 sequence of thirty virus clones was determined. Interestingly, the most common
254 mammalian adaptation determinants of PB2-E627K and PB2-D701N (27, 28), did not
255 appear in any of the thirty clones, indicating that other viable adaptations were present
256 in the BJ27-MA virus. Here, five conserved amino acid mutations that could be linked
257 to increased pathogenicity were identified in 3 virus segments of the BJ27-MA virus
258 as PB2-E158G, PB2-M631L, HA-G218E (H3 numbering), NA-K110E and
259 NA-S453I.

260 PB2-E158G mutation resides in the amino-terminal NP binding region (1–269aa)
261 (23), and PB2-M631L lies in the PB2-PB1 and PB2-NP interaction regions (25). HA
262 G218E is located near the 220-loop of the globular head HA1 domain (33).

NA-K110E and NA-S453I reside in the amino-terminal and carboxyl-terminal region of NA protein, respectively; both are located in the interface of tetrameric structure of NA protein (34).

PB2 and NA segments in BJ27-MA virus conferred increased pathogenicity and replication capacity in mice

To identify virus segments from the BJ27-MA virus that confer increased pathogenicity in mice, a series of recombinant viruses were generated by reverse genetic based on wild type BJ27 (rBJ27) and BJ27-MA (rBJ27-MA) viruses. Recombinant viruses rBJ27-PB2, rBJ27-HA and rBJ27-NA were constructed in rBJ27 virus background with the substituted segments of PB2, HA and NA, respectively, from the rBJ27-MA virus. Mice infected with recombinant viruses were monitored over 14 days for weight loss and survival rate. As shown in Fig. 2A and B, all of rBJ27 and rBJ27-HA viruses infected mice, similar to wild type BJ27 virus infection, survived with maximum 6.7% and 8.8% weight loss respectively. By contrast, mice infected with rBJ27-MA and rBJ27-PB2 viruses resulted in 25% to 31% weight loss and 100% mortality by 6 dpi. rBJ27-NA virus showed moderate increase in pathogenicity with 40% mortality. The MLD_{50} values also showed the same descending order of virus virulence: rBJ27-MA, rBJ27-PB2 (both MLD_{50}, 4.75 $\log_{10}$ $TCID_{50}$) > rBJ27-NA (5.75 $\log_{10}$ $TCID_{50}$) > rBJ27 and rBJ27-HA (>6.5 $\log_{10}$ $TCID_{50}$) (Table 1). None of these segment recombinants was neurotropic although they were recovered from lungs and extrapulmonary organs (kidney and/or spleen) (Table 1). Thus, the adaptive PB2 and NA segments of BJ27-MA conferred increased virulence in wild type BJ27 virus background in mice.

Combined PB2 and NA segments of BJ27-MA virus contributed to neurovirulence

Influenza virus replication in the central nervous system (CNS) often leads to fatal outcome (35-37). Although mouse-adapted BJ27-MA virus was able to efficiently replicate in murine brain, none of the above single segment recombinant viruses was found in the brain of infected mice (Table 1). Next, we generated three double-segment recombinant viruses based on the rBJ27 backbone: rBJ27-PB2/HA virus, rBJ27-PB2/NA virus and rBJ27-HA/NA virus. As shown in Table 2, only rBJ27-PB2/NA virus was recovered from infected murine brains at 3 and 5 dpi which produced MLD_{50} value and viral loads similar to those of rBJ27-MA virus at each time point. Viral NP was readily detected in neurons of mice infected separately with rBJ27-MA and rBJ27-PB2/NA viruses (Fig. 3A). These data demonstrated that the combined PB2 and NA segments of rBJ27-MA contributed to its neurovirulence in mice.

The ability of double segment recombinant viruses to replicate in neural tissue was assessed in mouse neuroblastoma N2a cells which has been used to study the replication of neurotropic viruses (38). Only rBJ27-MA and rBJ27-PB2/NA viruses showed up to 15-fold increased virus output relative to rBJ27 virus at 24 and/or 36 hpi (Fig. 3B). The other viruses (rBJ27-PB2/HA and rBJ27-HA/NA) showed no significant difference in virus titers at all time points. Therefore, the combined PB2 and NA segments also enhanced the replication of rBJ27-MA virus in neural cells.

PB2-M631L, PB2-E158G and NA-K110E contributed to severe BJ27-MA virus infection

To pinpoint the contribution of the single mutations in PB2 and NA to the increased

pathogenicity of BJ27-MA, four point mutant viruses were generated with the rBJ27 backbone as rBJ27-PB2/E158G, rBJ27-PB2/M631L, rBJ27-NA/K110E and rBJ27-NA/S453I viruses. Virus rBJ27-PB2/M631L was most virulent in that all infected mice died before 8 dpi (Fig. 2C and D). Virus rBJ27-PB2/E158G and rBJ27-NA/K110E caused moderate weight loss of around 13.3% without fatality. Virus NA-S453I and wild type rBJ27 were least pathogenic and caused little weight loss. MLD_{50} was highest with PB2-M631L virus (4.75 $\log_{10}$ $TCID_{50}$) relative to all the other viruses (>6.5 $\log_{10}$ $TCID_{50}$) (Table 1). Compared with rBJ27, the viral titers of rBJ27-PB2/M631L, rBJ27-PB2/E158G and rBJ27-NA/K110E in murine lungs were significantly higher at 3 and/or 5 dpi (Table 1). Virus rBJ27-PB2/M631L produced the highest virus titers. However, none of the four point mutation viruses showed extrapulmonary infection in liver, spleen, kidney or brain.

Histopathological findings of lung tissues taken at 5 dpi gave a severity picture that was similar to the pathogenicity results (Fig. 2E). Virus rBJ27-PB2/M631L and rBJ27-MA elicited the most severe lung lesions of edema, inflammatory infiltrates, interstitial pneumonia and bronchopneumonia. Lungs from rBJ27-PB2/E158G and rBJ27-NA/K110E virus infection showed less severe bronchopneumonic changes. Almost no lung lesion was detected from infection with rBJ27 and rBJ27-NA/S453I viruses except for some thickening of alveolar wall and mild infiltration of inflammatory cells.

We next compared the replication of the four mutant viruses in MDCK and A549 cells, infected at MOI of 0.01 or 0.1 respectively, over 72 h. In MDCK cells (Fig. 4A),

rBJ27-MA virus showed higher output (up to 56-fold higher) than the parental rBJ27 from 24 to 72 hpi, and PB2/M631L mutation increased the replication of rBJ27 virus at 36 hpi (both $P < 0.05$). Replication of rBJ27-PB2/E158G, rBJ27-NA/K110E and rBJ27-NA/S453I viruses was similar to that of rBJ27 virus. In A549 cells, the rBJ27-MA virus also showed higher output from 24 to 60 hpi, and rBJ27-PB2/M631L, rBJ27-PB2/E158G and rBJ27-NA/K110E viruses produced more progeny virus at 24 or 36 hpi than rBJ27 virus (all $P < 0.05$) (Fig. 4B). Therefore, in summary, PB2-M631L, PB2-E158G and NA-K110E mutations in rBJ27 virus backbone conferred more severe infection than wild type rBJ27 virus in mice and mammalian cells, with PB2-M631L mutation being the most potent determinant.

PB2-M631L and PB2-E158G mutations enhanced polymerase activity of BJ27-MA virus

PB2 is one of the components of ribonucleoprotein (RNP). RNP polymerase activity has been shown to catalyze viral transcription and genomic replication, which correlate with viral replication and pathogenicity in hosts (39). To evaluate whether the mutations of PB2-E158G and PB2-M631L affect viral polymerase activity, we generated two mutant RNP complexes under the background of the RNP of rBJ27, and measured their polymerase activities in 293T cells by a luciferase minigenome assay (Fig. 5). RNP polymerase activity with single E158G or M631L mutation was 28 or 62 times higher, respectively, than that of wild type rBJ27 RNP complex; combined E158G and M631L PB2 mutations induced 75 times higher activity than with the rBJ27 RNP complex (all $P < 0.05$). Western blotting, based on protein lysates

derived from 293T cells transfected with the different PB2 mutant plasmids in RNP polymerase assays, showed comparable PB2 protein expression, which indicated that the differences in polymerase activity were not due to levels of protein expression (Fig. 5). Collectively, the raised polymerase activity conferred by PB2-M631L and PB2-E158G mutations correlate with their severity of virus replication in mice and mammalian cells, and suggest that elevated polymerase activity, rather than protein, mediated the increased replication of BJ27-MA virus; the single M631L mutation in PB2 appeared as a major contributor.

NA-K110E increased NA enzymatic activity

NA enzymatic activity is associated with influenza virus replication and pathogenicity (40). The two amino acid mutations (K110E and S453I) in the BJ27-MA NA protein were evaluated for NA enzymatic activity as described previously (32). Based on K_m values, we found that the NA-K110E mutation caused a significant increase as did the mutant segment (rBJ27-NA with double mutations) in substrate affinity (Table 3). Similarly, V_{max}, which was determined by both the specific activity and the amount of enzyme in the reaction mixture, was significantly higher with the K110E mutation than with wild type rBJ27 virus ($P < 0.05$). The V_{max} of rBJ27-NA/S453I virus was increased but not significantly higher than rBJ27 virus. Thus, NA-K110E mutation improved NA enzymatic activity, which would have contributed to the increased replication and pathogenicity of rBJ27-MA virus in mice.

Discussion

In this study, serial passage of avian H10N7 virus in mice resulted in dramatic

376 acquisition of pathogenicity in terms of increase virus replication, virus dissemination
377 that extended to the brain and high mortality rate. Five conserved mutations were
378 identified in PB2, HA and NA genes of the passaged BJ27-MA virus (PB2-E158G,
379 PB2-M631L, HA-G218E, NA-K110E and NA-S453I). The mutations in PB2 and NA
380 genes significantly up-regulated viral polymerase activity and NA enzymatic activity
381 respectively; their combined presence in BJ27-MA virus was necessary for
382 neurovirulence. In particular, M631L mutation in PB2 was a major molecular
383 determinant for the overall increase in virulence of the mouse-adapted H10N7 virus.
384 PB2 gene plays important roles in the adaptation of influenza viruses from avian to
385 mammals through increasing polymerase activity and viral replication (41).
386 Polymerases of avian-origin generally have impaired function in human and other
387 mammalian cells (39). To overcome this natural restriction, avian polymerases need to
388 acquire mutations that lead to improved activity in mammalian hosts. E627K or
389 D701N in PB2 is a common adaptive change of avian influenza viruses that cause
390 mammals and human infections (27, 28, 42). In our mice adaptation study, in place of
391 these reported mutations in the PB2 gene, E158G and M631L were identified to
392 mediate the promotion of polymerase activity, virus pathogenicity and replication in
393 mice. PB2-E158G was reported to be a pathogenic determinant of pandemic H1N1
394 and avian H5 influenza viruses in mice (24). PB2-M631L is a novel and dominant
395 pathogenic mutation not previously described. The structure of PB2 shows that
396 position 631 is close to position 627 and located at the PB2-PB1 and PB2-NP
397 interaction regions (22). From the isolates of human infection cases, PB2 sequence

398 analysis found that nine avian H5N1 and two pandemic H1N1/2009 viruses possessed
399 PB2-M631L but not E627K or D701N mutation, implying that PB2-M631L could be
400 functionally important independent of E627K or D701N. Likewise, during the
401 pH1N1/2009 virus outbreak in humans, the PB2-E627K mutation was absent; instead
402 PB2-G590S/Q591R mutation was responsible for increased polymerase activity in
403 human cells (43). Therefore, PB2-M631L could be a novel functional mutation in
404 H10N7 virus adaptation in mammalian hosts.

405 NA cleaves sialic acid from glycans on host cell and emerging virions, thus
406 allowing unhindered release of progeny virus from infected cells (40). Several studies
407 found that amino acid mutations or deletions in NA can affect NA enzymatic activity,
408 which correlate with virus replication and pathogenicity *in vitro* or *in vivo* (44-46).
409 Here, NA-K110E in BJ27-MA virus, acting as a novel mammalian mutation,
410 significantly increased NA activity and viral replication in mice. We found that the
411 two NA mutations (K110E and S453I) are located in the interface of tetrameric
412 structure of NA (34) which may affect the formation of tetramer.

413 Neurovirulence is not commonly observed in the adaptation of avian influenza
414 viruses in mice (21-23, 42). Besides our H10N7 virus, another related virus (H10N8)
415 was reported to acquire neurotropism after two passages in mice (42), suggesting that
416 H10 subtype might be more able to gain the ability to replicate in mammalian brain.
417 Clinically, CNS disease is a common extra-respiratory complication in humans
418 induced by influenza virus. Patients with CNS manifestations are more likely to
419 experience severe illness (35-37). In Australian and Texas, USA, 9.7% and 8.8%

hospitalized children, respectively, infected with pH1N1/2009 virus had neurological complications (47, 48). Ying et al. also found that viruses with high replication ability in murine brain also possess high pathogenicity (49). The collective evidence indicates that high pathogenicity and neurovirulence could cooperate to promote fatalities in human cases of H10N8 virus infection. Molecular mechanism of influenza virus causing infection in the CNS is unclear. HA, NA and PB2 genes have been separately found to be critical to the neurovirulence of H1N1 or H5N1 viruses in mammalian hosts (50-53). However, in our present study, the viruses with single adapted PB2 or NA segment could not cause brain infection although when combined they replicated in the brain to a level comparable with rBJ27-MA virus which indicates that the synergistic effect of PB2 and NA is important for H10N7 neurovirulence.

In summary, our mouse adaptation study clearly shows that avian H10N7 virus can readily become highly virulent and neurotropic after limited passages in mice. We demonstrated that this enhanced pathogenicity was mediated by specific mutations in PB2 and NA genes; in particular PB2-M631L is a novel and critical determinant of virulence.

Acknowledgement

This work was supported by the National Key Research and Development Program (2016YFD0500204) and the National Key Technology R&D Program (2013BAD12B01).

Reference

1. **Palese P.** 2004. Influenza: old and new threats. Nat Med **10:**S82-87.

2. **Pu J, Wang S, Yin Y, Zhang G, Carter RA, Wang J, Xu G, Sun H, Wang M, Wen C, Wei Y, Wang D, Zhu B, Lemmon G, Jiao Y, Duan S, Wang Q, Du Q, Sun M, Bao J, Sun Y, Zhao J, Zhang H, Wu G, Liu J, Webster RG.** 2015. Evolution of the H9N2 influenza genotype that facilitated the genesis of the novel H7N9 virus. Proc Natl Acad Sci U S A **112:**548-553.

3. **Imai M, Watanabe T, Hatta M, Das SC, Ozawa M, Shinya K, Zhong G, Hanson A, Katsura H, Watanabe S.** 2012. Experimental adaptation of an influenza H5 HA confers respiratory droplet transmission to a reassortant H5 HA/H1N1 virus in ferrets. Nature **486:**420-428.

4. **Gao R, Cao B, Hu Y, Feng Z, Wang D, Hu W, Chen J, Jie Z, Qiu H, Xu K, Xu X, Lu H, Zhu W, Gao Z, Xiang N, Shen Y, He Z, Gu Y, Zhang Z, Yang Y, Zhao X, Zhou L, Li X, Zou S, Zhang Y, Li X, Yang L, Guo J, Dong J, Li Q, Dong L, Zhu Y, Bai T, Wang S, Hao P, Yang W, Zhang Y, Han J, Yu H, Li D, Gao GF, Wu G, Wang Y, Yuan Z, Shu Y.** 2013. Human infection with a novel avian-origin influenza A (H7N9) virus. N Engl J Med **368:**1888-1897.

5. **Chen H, Yuan H, Gao R, Zhang J, Wang D, Xiong Y, Fan G, Yang F, Li X, Zhou J, Zou S, Yang L, Chen T, Dong L, Bo H, Zhao X, Zhang Y, Lan Y, Bai T, Dong J, Li Q, Wang S, Zhang Y, Li H, Gong T, Shi Y, Ni X, Li J, Zhou J, Fan J, Wu J, Zhou X, Hu M, Wan J, Yang W, Li D, Wu G, Feng**

Z, Gao GF, Wang Y, Jin Q, Liu M, Shu Y. 2014. Clinical and epidemiological characteristics of a fatal case of avian influenza A H10N8 virus infection: a descriptive study. Lancet **383:**714-721.

6. **Vachieri SG, Xiong X, Collins PJ, Walker PA, Martin SR, Haire LF, Zhang Y, McCauley JW, Gamblin SJ, Skehel JJ.** 2014. Receptor binding by H10 influenza viruses. Nature **511:**475-477.

7. **Zhang W, Wan J, Qian K, Liu X, Xiao Z, Sun J, Zeng Z, Wang Q, Zhang J, Jiang G, Nie C, Jiang R, Ding C, Li R, Horby P, Gao Z.** 2014. Clinical characteristics of human infection with a novel avian-origin influenza A(H10N8) virus. Chin Med J (Engl) **127:**3238-3242.

8. **Feldmann H, Kretzschmar E, Klingeborn B, Rott R, Klenk HD, Garten W.** 1988. The structure of serotype H10 hemagglutinin of influenza A virus: comparison of an apathogenic avian and a mammalian strain pathogenic for mink. Virology **165:**428-437.

9. **Englund L, Hard af Segerstad C.** 1998. Two avian H10 influenza A virus strains with different pathogenicity for mink (Mustela vison). Arch Virol **143:**653-666.

10. **Wu H, Lu R, Wu X, Peng X, Xu L, Cheng L, Lu X, Jin C, Xie T, Yao H, Wu N.** 2015. Novel reassortant H10N7 avian influenza viruses isolated from chickens in Eastern China. J Clin Virol **65:**58-61.

11. **Vijaykrishna D, Deng YM, Su YC, Fourment M, Iannello P, Arzey GG, Hansbro PM, Arzey KE, Kirkland PD, Warner S, O'Riley K, Barr IG,**

Smith GJ, Hurt AC. 2013. The recent establishment of North American H10 lineage influenza viruses in Australian wild waterfowl and the evolution of Australian avian influenza viruses. J Virol **87:**10182-10189.

12. **Arzey GG, Kirkland PD, Arzey KE, Frost M, Maywood P, Conaty S, Hurt AC, Deng YM, Iannello P, Barr I, Dwyer DE, Ratnamohan M, McPhie K, Selleck P.** 2012. Influenza virus A (H10N7) in chickens and poultry abattoir workers, Australia, 2012/04/21 ed, vol 18, p 814-816.

13. **Berg M, Englund L, Abusugra IA, Klingeborn B, Linne T.** 1990. Close relationship between mink influenza (H10N4) and concomitantly circulating avian influenza viruses. Arch Virol **113:**61-71.

14. **Wang N, Zou W, Yang Y, Guo X, Hua Y, Zhang Q, Zhao Z, Jin M.** 2012. Complete genome sequence of an H10N5 avian influenza virus isolated from pigs in central China. J Virol **86:**13865-13866.

15. **Su S, Qi W, Zhou P, Xiao C, Yan Z, Cui J, Jia K, Zhang G, Gray GC, Liao M, Li S.** 2014. First evidence of H10N8 Avian influenza virus infections among feral dogs in live poultry markets in Guangdong province, China. Clin Infect Dis **59:**748-750.

16. **Zohari S, Neimanis A, Harkonen T, Moraeus C, Valarcher JF.** 2014. Avian influenza A(H10N7) virus involvement in mass mortality of harbour seals (Phoca vitulina) in Sweden, March through October 2014. Euro Surveill **19**.

17. **Bodewes R, Bestebroer TM, van der Vries E, Verhagen JH, Herfst S,**

Koopmans MP, Fouchier RA, Pfankuche VM, Wohlsein P, Siebert U, Baumgartner W, Osterhaus AD. 2015. Avian Influenza A(H10N7) virus-associated mass deaths among harbor seals. Emerg Infect Dis **21:**720-722.

18. **Krog JS, Hansen MS, Holm E, Hjulsager CK, Chriel M, Pedersen K, Andresen LO, Abildstrom M, Jensen TH, Larsen LE.** 2015. Influenza A(H10N7) virus in dead harbor seals, Denmark. Emerg Infect Dis **21:**684-687.

19. Pan American Health Organization 2004. Avian influenza virus A (H10N7) circulating among humans in Egypt. http://www.paho.org/hq/dmdocuments/2010/Avian_Influenza_Egypt_070503.pdf.

20. **Kayali G, Ortiz EJ, Chorazy ML, Gray GC.** 2010. Evidence of previous avian influenza infection among US turkey workers. Zoonoses Public Health **57:**265-272.

21. **Brown EG, Liu H, Kit LC, Baird S, Nesrallah M.** 2001. Pattern of mutation in the genome of influenza A virus on adaptation to increased virulence in the mouse lung: identification of functional themes. Proc Natl Acad Sci U S A **98:**6883-6888.

22. **Keleta L, Ibricevic A, Bovin NV, Brody SL, Brown EG.** 2008. Experimental evolution of human influenza virus H3 hemagglutinin in the mouse lung identifies adaptive regions in HA1 and HA2. J Virol **82:**11599-11608.

530 23. **Ping J, Dankar SK, Forbes NE, Keleta L, Zhou Y, Tyler S, Brown EG.**
531 2010. PB2 and hemagglutinin mutations are major determinants of host range
532 and virulence in mouse-adapted influenza A virus. J Virol **84:**10606-10618.
533 24. **Zhou B, Li Y, Halpin R, Hine E, Spiro DJ, Wentworth DE.** 2011. PB2
534 residue 158 is a pathogenic determinant of pandemic H1N1 and H5 influenza
535 a viruses in mice. J Virol **85:**357-365.
536 25. **Wang J, Sun Y, Xu Q, Tan Y, Pu J, Yang H, Brown EG, Liu J.** 2012.
537 Mouse-adapted H9N2 influenza A virus PB2 protein M147L and E627K
538 mutations are critical for high virulence. PLoS One **7:**e40752.
539 26. **Tan L, Su S, Smith DK, He S, Zheng Y, Shao Z, Ma J, Zhu H, Zhang G.**
540 2014. A combination of HA and PA mutations enhances virulence in a
541 mouse-adapted H6N6 influenza A virus. J Virol **88:**14116-14125.
542 27. **Gao Y, Zhang Y, Shinya K, Deng G, Jiang Y, Li Z, Guan Y, Tian G, Li Y,**
543 **Shi J, Liu L, Zeng X, Bu Z, Xia X, Kawaoka Y, Chen H.** 2009.
544 Identification of amino acids in HA and PB2 critical for the transmission of
545 H5N1 avian influenza viruses in a mammalian host. PLoS Pathog **5:**e1000709.
546 28. **Yamayoshi S, Fukuyama S, Yamada S, Zhao D, Murakami S, Uraki R,**
547 **Watanabe T, Tomita Y, Neumann G, Kawaoka Y.** 2015. Amino acids
548 substitutions in the PB2 protein of H7N9 influenza A viruses are important for
549 virulence in mammalian hosts. Sci Rep **5:**8039.
550 29. **Reed LJ, Muench HA.** 1938. A Simple Method of Estimating Fifty Per Cent
551 Endpoints. Am J Epidemiol **27:** 493–497.

552 30. **Ilyushina NA, Khalenkov AM, Seiler JP, Forrest HL, Bovin NV, Marjuki**
553 **H, Barman S, Webster RG, Webby RJ.** 2010. Adaptation of pandemic
554 H1N1 influenza viruses in mice. J Virol **84:**8607-8616.
555 31. **Sun Y, Qin K, Wang J, Pu J, Tang Q, Hu Y, Bi Y, Zhao X, Yang H, Shu**
556 **Y, Liu J.** 2011. High genetic compatibility and increased pathogenicity of
557 reassortants derived from avian H9N2 and pandemic H1N1/2009 influenza
558 viruses. Proc Natl Acad Sci U S A **108:**4164-4169.
559 32. **Potier M, Mameli L, Belisle M, Dallaire L, Melancon SB.** 1979.
560 Fluorometric assay of neuraminidase with a sodium
561 (4-methylumbelliferyl-alpha-D-N-acetylneuraminate) substrate. Anal Biochem
562 **94:**287-296.
563 33. **Wang M, Zhang W, Qi J, Wang F, Zhou J, Bi Y, Wu Y, Sun H, Liu J,**
564 **Huang C, Li X, Yan J, Shu Y, Shi Y, Gao GF.** 2015. Structural basis for
565 preferential avian receptor binding by the human-infecting H10N8 avian
566 influenza virus. Nat Commun **6:**5600.
567 34. **Sun X, Li Q, Wu Y, Wang M, Liu Y, Qi J, Vavricka CJ, Gao GF.** 2014.
568 Structure of influenza virus N7: the last piece of the neuraminidase "jigsaw"
569 puzzle. J Virol **88:**9197-9207.
570 35. **Mizuguchi M, Yamanouchi H, Ichiyama T, Shiomi M.** 2007. Acute
571 encephalopathy associated with influenza and other viral infections. Acta
572 Neurol Scand Suppl **186:**45-56.
573 36. **McSwiney P, Purnama J, Kornberg A, Danchin M.** 2014. A severe

574 neurological complication of influenza in a previously well child. BMJ Case
575 Rep **2014**.
576 37. **Tanaka H, Park CH, Ninomiya A, Ozaki H, Takada A, Umemura T, Kida**
577 **H.** 2003. Neurotropism of the 1997 Hong Kong H5N1 influenza virus in mice.
578 Vet Microbiol **95:**1-13.
579 38. **Sajjanar B, Saxena S, Bisht D, Singh AK, Reddy GM, Singh R, Singh R,**
580 **Kumar S.** 2016. Effect of nicotinic acetylcholine receptor alpha 1 (nAChRα1)
581 peptides on rabies virus infection in neuronal cells. Neuropeptides **57:**59-64.
582 39. **Xu G, Zhang X, Gao W, Wang C, Wang J, Sun H, Sun Y, Guo L, Zhang**
583 **R, Chang K-C.** 2016. Prevailing PA mutation K356R in avian influenza
584 H9N2 virus increases mammalian replication and pathogenicity. Journal of
585 Virology **90:**8105-8114.
586 40. **Colman PM.** 1994. Influenza virus neuraminidase: structure, antibodies, and
587 inhibitors. Protein Sci **3:**1687-1696.
588 41. **Fan S, Hatta M, Kim JH, Halfmann P, Imai M, Macken CA, Le MQ,**
589 **Nguyen T, Neumann G, Kawaoka Y.** 2014. Novel residues in avian
590 influenza virus PB2 protein affect virulence in mammalian hosts. Nat
591 Commun **5:**5021.
592 42. **Zhou B, Pearce MB, Li Y, Wang J, Mason RJ, Tumpey TM, Wentworth**
593 **DE.** 2013. Asparagine substitution at PB2 residue 701 enhances the replication,
594 pathogenicity, and transmission of the 2009 pandemic H1N1 influenza A virus.
595 PLoS One **8:**e67616.

596 43. **Mehle A, Doudna JA.** 2009. Adaptive strategies of the influenza virus
597 polymerase for replication in humans. Proc Natl Acad Sci U S A
598 **106:**21312-21316.
599 44. **Sun Y, Tan Y, Wei K, Sun H, Shi Y, Pu J, Yang H, Gao GF, Yin Y, Feng**
600 **W, Perez DR, Liu J.** 2013. Amino Acid 316 of Hemagglutinin and the
601 Neuraminidase Stalk Length Influence Virulence of H9N2 Influenza Virus in
602 Chickens and Mice. J Virol **87:**2963-2968.
603 45. **Hossain MJ, Hickman D, Perez DR.** 2008. Evidence of expanded host range
604 and mammalian-associated genetic changes in a duck H9N2 influenza virus
605 following adaptation in quail and chickens. PLoS One **3:**e3170.
606 46. **Chen H, Bright RA, Subbarao K, Smith C, Cox NJ, Katz JM, Matsuoka**
607 **Y.** 2007. Polygenic virulence factors involved in pathogenesis of 1997 Hong
608 Kong H5N1 influenza viruses in mice. Virus Res **128:**159-163.
609 47. **Wilking AN, Elliott E, Garcia MN, Murray KO, Munoz FM.** 2014. Central
610 nervous system manifestations in pediatric patients with influenza A H1N1
611 infection during the 2009 pandemic. Pediatr Neurol **51:**370-376.
612 48. **Khandaker G, Zurynski Y, Buttery J, Marshall H, Richmond PC, Dale**
613 **RC, Royle J, Gold M, Snelling T, Whitehead B, Jones C, Heron L,**
614 **McCaskill M, Macartney K, Elliott EJ, Booy R.** 2012. Neurologic
615 complications of influenza A(H1N1)pdm09: surveillance in 6 pediatric
616 hospitals. Neurology **79:**1474-1481.
617 49. **Zhang Y, Zhang Q, Kong H, Jiang Y, Gao Y, Deng G, Shi J, Tian G, Liu**

L, Liu J. 2013. H5N1 hybrid viruses bearing 2009/H1N1 virus genes transmit in guinea pigs by respiratory droplet. Science **340:**1459-1463.

50. **Yen HL, Aldridge JR, Boon AC, Ilyushina NA, Salomon R, Hulse-Post DJ, Marjuki H, Franks J, Boltz DA, Bush D, Lipatov AS, Webby RJ, Rehg JE, Webster RG.** 2009. Changes in H5N1 influenza virus hemagglutinin receptor binding domain affect systemic spread. Proc Natl Acad Sci U S A **106:**286-291.

51. **Sun X, Tse LV, Ferguson AD, Whittaker GR.** 2010. Modifications to the hemagglutinin cleavage site control the virulence of a neurotropic H1N1 influenza virus. J Virol **84:**8683-8690.

52. **Shinya K, Hamm S, Hatta M, Ito H, Ito T, Kawaoka Y.** 2004. PB2 amino acid at position 627 affects replicative efficiency, but not cell tropism, of Hong Kong H5N1 influenza A viruses in mice. Virology **320:**258-266.

53. **Goto H, Wells K, Takada A, Kawaoka Y.** 2001. Plasminogen-binding activity of neuraminidase determines the pathogenicity of influenza A virus. J Virol **75:**9297-9301.

640 **Figure legends**

641 **FIG 1** Pathogenicity and replication of wild type (BJ27) and mouse-adapted
642 (BJ27-MA) H10N7 viruses in mice. Six-week-old female BALB/c mice were
643 inoculated with $10^{5.5}$ $TCID_{50}$ of the indicated viruses or mock infected with PBS. (A)
644 Body weight changes over a 14-day period were plotted as percentage of body weight
645 at 0 dpi (n = 5 per group). Data are presented as means ± SD of five individual mice.
646 (B) Survival data expressed as percentage of mice infected with indicated virus. Mice
647 that lost > 30% of their baseline weight were euthanized. BJ27 and BJ27-MA virus
648 titers were determined in lungs (C) and brains (D) of infected mice (n = 3 per group).
649 Data are presented as means ± SD of three individual mice. ＊, the value is
650 significantly different from that of BJ27 ($P < 0.05$, ANOVA).

651

652 **FIG 2** Relative virulence of different recombinant and mutant BJ27 (H10N7) viruses
653 in mice. (A and C) Body weight changes in mice (n = 5) infected with $10^{5.5}$ $TCID_{50}$ of
654 indicated viruses over a 14-day period, plotted as percentage of body weight at 0 dpi.
655 Data are presented as means ± SD of five individual mice. (B and D) Survival data
656 expressed as percentage of mice infected with indicated viruses. Mice that lost more
657 than 30% of baseline weight were euthanized. (E) H&E examination was performed
658 on the lungs of mice infected with indicated viruses at 5 dpi. Virus rBJ27-PB2/M631L
659 and rBJ27-MA infection caused severe bronchopneumonia; rBJ27-PB2/E158G and
660 rBJ27-NA/K110E infections produced moderate bronchopneumonia； rBJ27 and
661 rBJ27-NA/S453I infection caused almost no lung lesion. Scale bar, 200 μm.

662 **FIG 3** Neurovirulence of recombinant BJ27 (H10N7) viruses. (A) Sections of brains
663 taken from mice 5 dpi with $10^{5.5}$ $TCID_{50}$ of indicated viruses were immunostained for
664 viral NP (open arrow). Scale bar, 400 μm. (B) Growth kinetics of recombinant viruses
665 in neuronal N2a cells. Confluent N2a cells were infected with indicated viruses at 0.1
666 MOI. Data are presented as means ± SD of three independent experiments. ＊, the
667 value is significantly different from that of rBJ27 ($P < 0.05$, ANOVA).
668
669 **FIG 4** Growth kinetics of recombinant H10N7 viruses in MDCK and A549 cells.
670 Confluent MDCK (A) or A549 (B) cells were infected with viruses as indicated at
671 MOI of 0.01 or 0.1 respectively. Data are presented as means ± SD of three
672 independent experiments. ＊, the value is significantly different from that of rBJ27 (P
673 < 0.05, ANOVA).
674
675 **FIG 5** Polymerase activity of BJ27 with different PB2 mutations in minigenome
676 assays. Luciferase activities were relative to wild type BJ27 set at 100%. Expression
677 of PB2 and β-actin was detected by Western blotting. Data are presented as means ±
678 SD of three independent experiments. ＊, the value is significantly different from that
679 of BJ27 ($P < 0.05$, ANOVA).

TABLE 1 Pathogenicity and replication of BJ27 (H10N7) recombinant and mutant viruses in mice

Virus	MLD_{50} (log_{10} $TCID_{50}$)	Average virus titer in sample [a]									
		Lung		Brain		Spleen		Kidney		Liver	
		3 dpi	5 dpi	3 dpi	5 dpi	3 dpi	5 dpi	3 dpi	5 dpi	3 dpi	5 dpi
rBJ27	>6.5	4.5±0.3	4.7±0.1	0/3 [b]	0/3	0/3	0/3	0/3	0/3	0/3	0/3
rBJ27-MA	4.75	6.5±0.3*	6.9±0.3*	2.1±0.4*	2.8±0.6*	2.3,1.8 [c]*	2.3,1.8*	0/3	2.9±0.3*	0/3	0/3
rBJ27-PB2	4.75	6.2±0.4*	6.6±0.3*	0/3	0/3	2.3*	0/3	0/3	2.2±0.6*	0/3	0/3
rBJ27-HA	>6.5	5.0±0.4	5.4±0.3	0/3	0/3	0/3	0/3	0/3	0/3	0/3	0/3
rBJ27-NA	5.75	5.5±0.1*	6.1±0.3*	0/3	0/3	1.8*	0/3	0/3	0/3	0/3	0/3
rBJ27-PB2/E158G	>6.5	5.2±0.4*	5.5±0.3*	0/3	0/3	0/3	0/3	0/3	0/3	0/3	0/3
rBJ27-PB2/M631L	4.75	5.7±0.1*	6.3±0.1*	0/3	0/3	0/3	0/3	0/3	0/3	0/3	0/3
rBJ27-NA/K110E	>6.5	5.2±0.3*	5.3±0.4	0/3	0/3	0/3	0/3	0/3	0/3	0/3	0/3
rBJ27-NA/S453I	>6.5	4.9±0.4	5.3±0.1	0/3	0/3	0/3	0/3	0/3	0/3	0/3	0/3

[a] Mean virus titer in sample (log_{10} $TCID_{50}$/ml) ± SD. The lower limit of detection was $10^{0.75}$ $TCID_{50}$/ml for each sample. *, virus titer of corresponding strains was significantly higher than that of rBJ27 ($P < 0.05$, ANOVA).

[b] The number of samples with recovered viruses versus the number of total collected samples.

[c] The number(s) shows the virus titer in an individual infected mouse.

TABLE 2 Pathogenicity and replication of double-segment recombinant H10N7 viruses in murine brain

Virus	MLD_{50}	Average virus titer in brain [a]	
		3 dpi	5 dpi
rBJ27	>6.5	0/3 [b]	0/3
rBJ27-MA	4.75	2.1±0.4	2.8±0.6
rBJ27-PB2/HA	5.25	0/3	0/3
rBJ27-PB2/NA	4.75	1.8,2.3 [c]	2.5±0.5
rBJ27-HA/NA	5.5	0/3	0/3

[a] Mean virus titer in sample (log_{10} $TCID_{50}$/ml) ± SD. Lower limit of detection was $10^{0.75}$ $TCID_{50}$/ml in the brain.

[b] The number of samples with recovered viruses versus the number of total collected samples.

[c] The number(s) shows virus titer in an individual mouse.

TABLE 3 NA enzyme kinetics of mutant H10N7 viruses [a]

Virus	K_m (μM)	V_{max}	V_{max} ratio [b]
rBJ27	28.7±4.1	0.53±0.10	1.00
rBJ27-MA	14.8±1.8*	0.90±0.09*	1.70*
rBJ27-NA	15.6±2.3*	0.86±0.06*	1.62*
rBJ27-NA/K110E	17.8±1.5*	0.78±0.02*	1.47*
rBJ27-NA/S453I	20.7±2.2	0.66±0.14	1.25

[a] A standardized virus dose of 10^6 $TCID_{50}$/ml was used for the NA kinetics assay. The enzyme kinetics data (standard deviation) were fit to the Michaelis-Menten equation by nonlinear regression to determine the Michaelis constant (K_m) and maximum velocity (V_{max}) of substrate conversion (in fluorescent units per second). * , the value of corresponding strains was significantly different from that of rBJ27 ($P < 0.05$, ANOVA).

[b] The ratio of the recombinant viruses versus rH10N7 virus V_{max} values.

Figure legends

Fig. 1

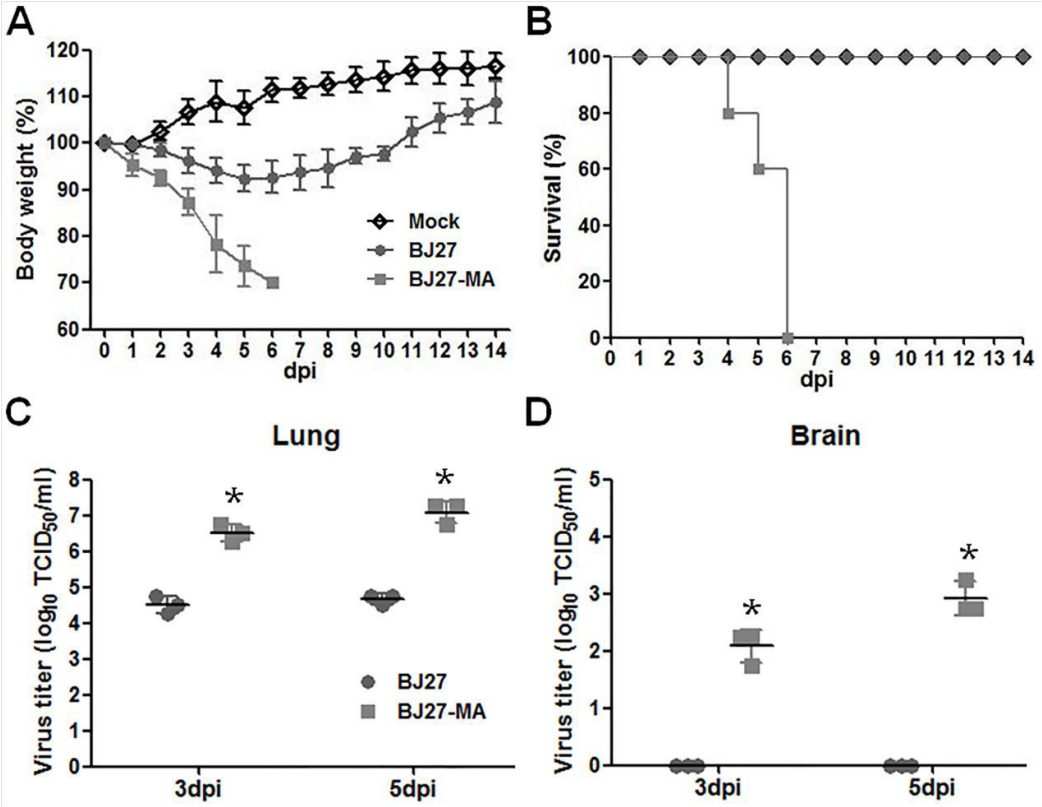

FIG 1 Pathogenicity and replication of wild type (BJ27) and mouse-adapted (BJ27-MA) H10N7 viruses in mice. Six-week-old female BALB/c mice were inoculated with $10^{5.5}$ $TCID_{50}$ of the indicated viruses or mock infected with PBS. (A) Body weight changes over a 14-day period were plotted as percentage of body weight at 0 dpi (n = 5 per group). Data are presented as means ± SD of five individual mice. (B) Survival data expressed as percentage of mice infected with indicated virus. Mice that lost > 30% of their baseline weight were euthanized. BJ27 and BJ27-MA virus titers were determined in lungs (C) and brains (D) of infected mice (n = 3 per group). Data are presented as means ± SD of three individual mice. * , the value is significantly different from that of BJ27 ($P < 0.05$, ANOVA).

Fig. 2

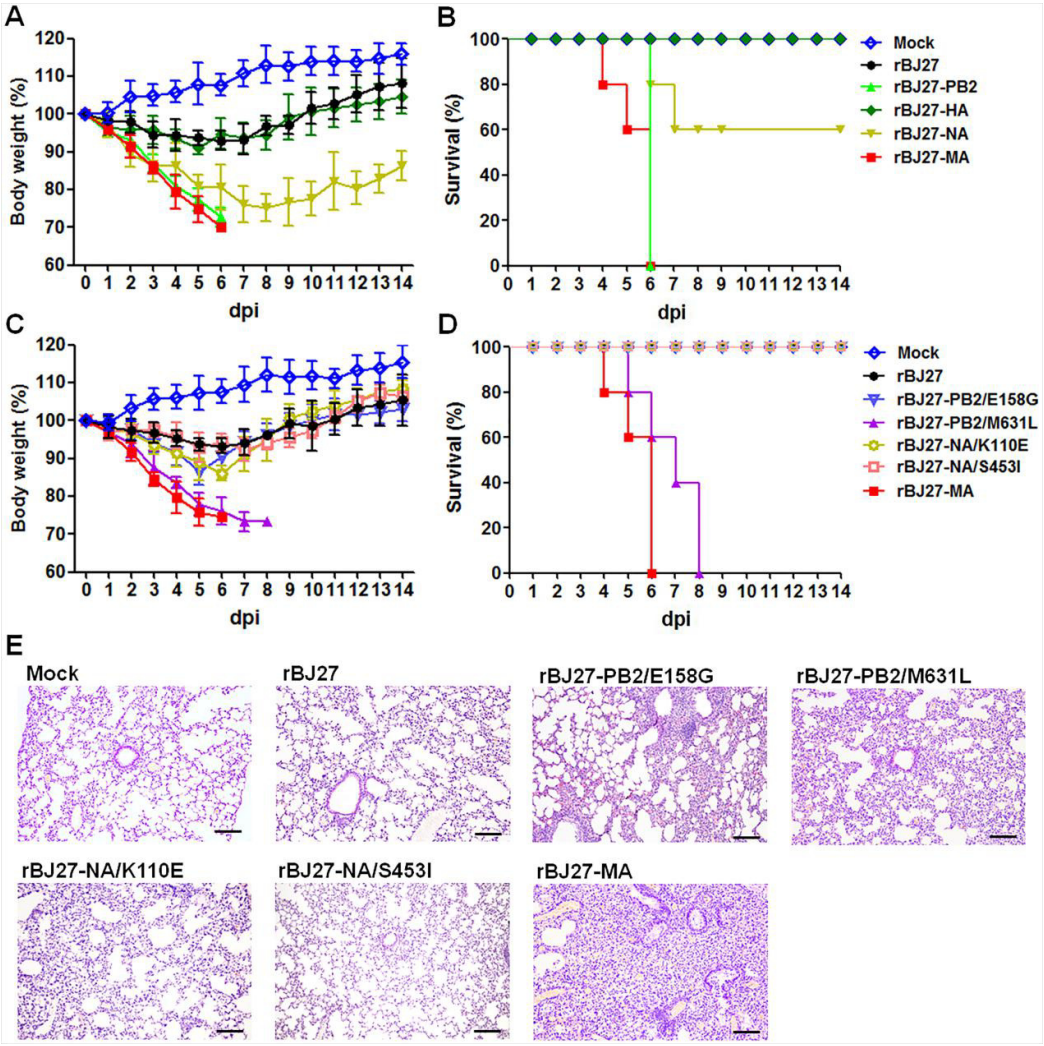

FIG 2 Relative virulence of different recombinant and mutant BJ27 (H10N7) viruses in mice. (A and C) Body weight changes in mice (n = 5) infected with $10^{5.5}$ $TCID_{50}$ of indicated viruses over a 14-day period, plotted as percentage of body weight at 0 dpi. Data are presented as means ± SD of five individual mice. (B and D) Survival data expressed as percentage of mice infected with indicated viruses. Mice that lost more than 30% of baseline weight were euthanized. (E) H&E examination was performed on the lungs of mice infected with indicated viruses at 5 dpi. Virus rBJ27-PB2/M631L and rBJ27-MA infection caused severe bronchopneumonia; rBJ27-PB2/E158G and rBJ27-NA/K110E infections produced moderate bronchopneumonia; rBJ27 and rBJ27-NA/S453I infection caused almost no lung lesion. Scale bar, 200 μm.

Fig. 3

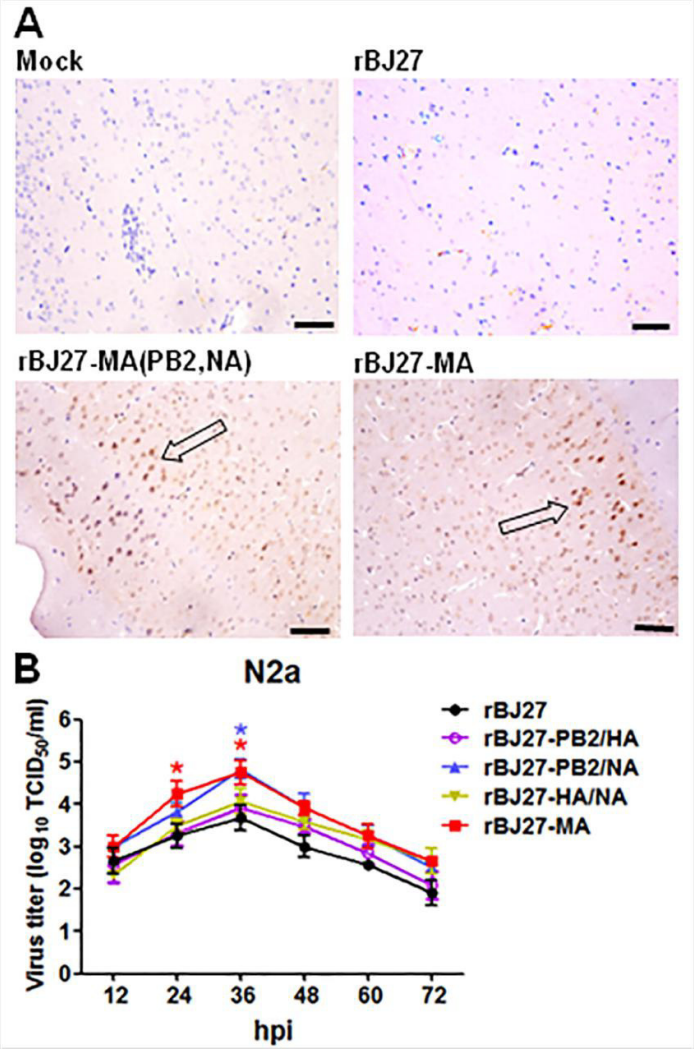

FIG 3 Neurovirulence of recombinant BJ27 (H10N7) viruses. (A) Sections of brains taken from mice at 5 dpi were immunostained for viral NP (open arrow). Scale bar, 400 μm. (B) Growth kinetics of recombinant viruses in neuronal N2a cells. Confluent N2a cells were infected with indicated viruses at 0.1 MOI. Data are presented as means ± SD of three independent experiments. ＊, the value is significantly different from that of rBJ27 ($P < 0.05$, ANOVA).

Fig. 4

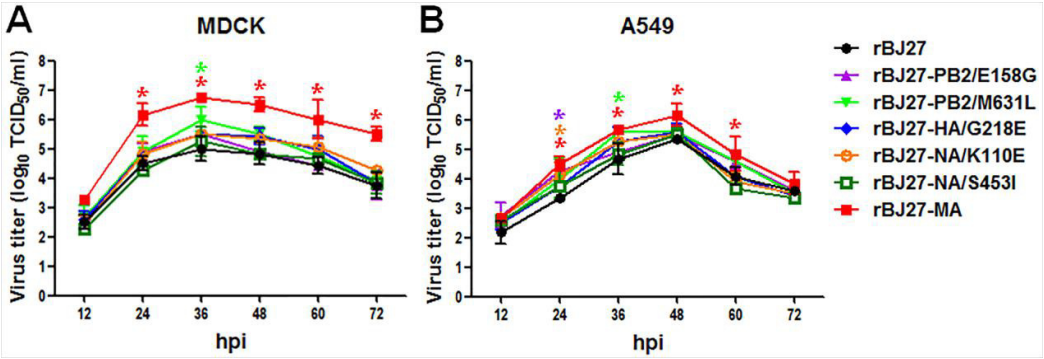

FIG 4 Growth kinetics of recombinant H10N7 viruses in MDCK and A549 cells. Confluent MDCK (A) or A549 (B) cells were infected with viruses as indicated at MOI of 0.01 or 0.1 respectively. Data are presented as means ± SD of three independent experiments. ＊, the value is significantly different from that of rBJ27 ($P < 0.05$, ANOVA).

Fig. 5

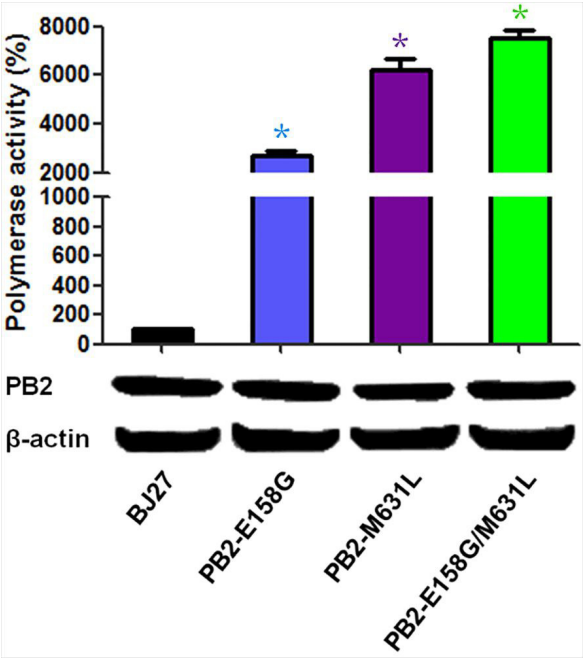

FIG 5 Polymerase activity of BJ27 with different PB2 mutations in minigenome assays. Luciferase activities were relative to wild type BJ27 set at 100%. Expression of PB2 and β-actin was detected by Western blotting. Data are presented as means ± SD of three independent experiments. ＊, the value is significantly different from that of BJ27 ($P < 0.05$, ANOVA).